

Study of Ξ^- hypernuclei in the Skyrme-Hartree-Fock approach

Yun Jin (金芸), Xian-Rong Zhou (周先荣),* and Yi-Yuan Cheng (程奔源)

School of Physics and Materials Science, East China Normal University, Shanghai 200241, P. R. China

H.-J. Schulze

INFN Sezione di Catania, Dipartimento di Fisica, Università di Catania, Via Santa Sofia 64, 95123 Catania, Italy

The properties of Ξ^- hypernuclei are studied systematically using a two-dimensional Skyrme-Hartree-Fock approach combined with three different ΞN Skyrme forces fitted to reproduce the existing data. We explore the impurity effect of a single Ξ^- hyperon on the radii, deformations, and density distributions of the nuclear core and point out qualitative differences between the different forces. We find that the Ξ^- removal energy of ${}^{13}_{\Xi p}\text{B}$ [${}^{12}\text{C}(\text{g.s.})+\Xi^-(1p)$] calculated by the SLX3 force is 0.7 MeV, which is in good agreement with a possible value of 0.82 ± 0.17 MeV from the KEK E176 experiment. The theoretical prediction for this weakly bound state depends strongly on the deformation of the nuclear core, which is analyzed in detail.

I. INTRODUCTION

Hypernuclei are an important aspect of the study of nuclear structure. In the past few decades, the investigation of hypernuclear structure has quickly developed into a new and broad field [1]. The motivation is to obtain clear and useful information on the YN and YY interactions, which are applied in astrophysics, for example [2]. In 1953, the first Λ hypernuclei were found in the laboratory [3]. Apart from Λ hypernuclei with the strangeness number $S = -1$, there are also other hypernuclei, such as Σ hypernuclei ($S = -1$) and Ξ^- hypernuclei ($S = -2$), which are, however, much more difficult to produce in scattering experiments. Therefore, only few experimental data of Ξ^- hypernuclei are so far available. The experiments for hypernuclei were conducted early at some large experimental research facilities, such as KEK and DAΦNE. Currently, there are several proposals for the measurement of Ξ^- hypernuclei and Ξ^- atoms by new and upgraded technologies at J-PARC [4, 5].

Early emulsion experiments [6, 7] reported possible Ξ^- removal energies for the hypernucleus ${}^{13}_{\Xi}\text{B}$ [${}^{12}\text{C}+\Xi^-$] as $3.70^{+0.18}_{-0.19}$, $0.62^{+0.18}_{-0.19}$, or $2.66^{+0.18}_{-0.19}$ MeV, but it is difficult to confirm that this observation is a bound Ξ^- hypernucleus due to a lack of precise identification. Recently, there are new events on the ${}^{13}_{\Xi}\text{B}$ hypernucleus reported by the KEK E176 collaboration [8]. A possible interpreted Ξ^- removal energy is $B_{\Xi} = 0.82 \pm 0.17$ MeV [9]. It is expected to be consistent with a decay from the ${}^{12}\text{C}+\Xi^-$ system at the $2P$ state, but this has not been confirmed.

Another experiment studied the production of the Ξ^- hypernuclei ${}^{12}_{\Xi}\text{Be}$ [${}^{11}\text{B}+\Xi^-$] by the (K^-, K^+) reaction [10], which was interpreted by fitting a Ξ^- -nucleus Woods-Saxon potential with a depth of about 14 MeV. Using this assumption, theoretical calculations [11, 12] predicted values of about 4–5 MeV for the ground-state Ξ^- removal energy.

In 2015, the important “Kiso” event was produced by the E373 experiment at KEK-PS [9] in the reaction process $\Xi^- + {}^{14}\text{N} \rightarrow {}^{15}_{\Xi}\text{C} \rightarrow {}^{10}_{\Lambda}\text{Be} + {}^5_{\Lambda}\text{He}$. This observation is the first

clear evidence of a deeply bound state of ${}^{15}_{\Xi}\text{C}$. A possible interpretation of the event is the creation of the p -state hypernucleus ${}^{15}_{\Xi p}\text{C}$ [${}^{14}\text{N}(\text{g.s.})+\Xi^-(1p)$] with a value of the Ξ^- removal energy $B_{\Xi} = 1.11 \pm 0.25$ MeV [13]. This interpretation was shown to be consistent with the production of ${}^{12}_{\Xi s}\text{Be}$ [10] within theoretical calculations in the Skyrme Hartree-Fock (SHF) and relativistic mean field (RMF) approaches [14]. It is also compatible with the one-peak interpretation of the preliminary analysis of ${}^{12}_{\Xi s}\text{Be}$ production in the J-PARC E05 experiment [15]. The strongly attractive nature of the XNI has also recently been confirmed by the latest experimental analysis on proton- Ξ^- correlations performed by the ALICE Collaboration [16].

Due to insufficient experimental information on the ΞN interaction (XNI), it is important to study Ξ^- hypernuclei in different theoretical approaches [17]: Within the framework of the cluster model, the light hypernucleus ${}^{12}_{\Xi}\text{Be}$ was calculated based on the assumption of an effective Ξ^- potential whose depth is about 14 MeV. It was predicted that the Ξ^- removal energy of the ${}^{12}_{\Xi}\text{Be}$ ground state is about 5 MeV and 2.2 MeV, with/out the ΞN Coulomb interaction, respectively [11]. The RMF method performed studies on spherical Ξ^- hypernuclei, such as ${}^{17}_{\Xi}\text{N}$, ${}^{41}_{\Xi}\text{K}$, ${}^{91}_{\Xi}\text{Y}$, ${}^{209}_{\Xi}\text{Ti}$, etc. [18–20], where it was found that the Ξ^- binding energies increase with the mass number of hypernuclei and that the ΞN Coulomb interaction makes the hyperon potential much deeper. Within the quark-mean-field approach, systematic studies were performed on Ξ^- hypernuclei from ${}^{12}_{\Xi}\text{Be}$ to ${}^{209}_{\Xi}\text{Ti}$ [21]. The XNI parameters were determined under the assumption of a Ξ^- potential depth at saturation density $U_{\Xi} = -12$ or -9 MeV. In the framework of a one-dimensional (1D) SHF model, three different XNIs SLX0, SLX2, SLX3 were proposed in [14] to reproduce in a consistent manner the experimental data for ${}^{12}_{\Xi}\text{Be}$ and ${}^{15}_{\Xi}\text{C}$ discussed above.

In this work we continue and extend the study of Ξ^- hypernuclei in a two-dimensional (2D) SHF model. One aim is to explore the impurity effect of a single Ξ^- hyperon on the deformation of core nuclei. We perform systematic calculations of Ξ^- hypernuclei from ${}^9_{\Xi}\text{Li}$ to ${}^{209}_{\Xi}\text{Ti}$, in particular for a series of hypernuclei with deformed cores from ${}^9_{\Xi}\text{Li}$ to ${}^{37}_{\Xi}\text{Cl}$. We focus on the Ξ^- binding energies, deformations, and nucleon and hyperon density distributions of Ξ^- hypernuclei, in

* Corresponding author: xrzhou@phy.ecnu.edu.cn

particular study the dependence of the theoretical predictions on the different XNIs SLX0, SLX2, SLX3.

The paper is organized as follows. In Sec. II we present the method of the self-consistent 2D SHF model and introduce the Skyrme forces for the effective XNI. Sec. III shows the results and discussion of deformations, binding energies, and nucleon and hyperon density distributions for Ξ^- hypernuclei from ${}^9_{\Xi}\text{Li}$ to ${}^{209}_{\Xi}\text{Ti}$. In Sec. IV, we summarize the paper.

II. FORMALISM

Our approach is the 2D SHF model, which is combined with a density-dependent Skyrme force for the XNI. In the self-consistent model, the total energy of a hypernucleus is calculated as [22–26]

$$E = \int d^3\mathbf{r} \varepsilon(\mathbf{r}), \quad \varepsilon = \varepsilon_{NN} + \varepsilon_{\Xi N} + \varepsilon_C, \quad (1)$$

where ε_{NN} is the energy density of the nucleon-nucleon interaction, $\varepsilon_{\Xi N}$ is the contribution due to the ΞN interaction, and ε_C is the energy density of the Coulomb interaction between protons and Ξ^- hyperon. These energy-density functionals are dependent on the one-body density ρ_q , kinetic density τ_q , and spin-orbit current \mathbf{J}_q ,

$$[\rho_q, \tau_q, \mathbf{J}_q] = \sum_{i=1}^{N_q} n_q^i \left[|\phi_q^i|^2, |\nabla\phi_q^i|^2, \phi_q^{i*} (\nabla\phi_q^i \times \boldsymbol{\sigma}) / i \right], \quad (2)$$

where ϕ_q^i ($i = 1, N_q$) are the self-consistently calculated single-particle (s.p.) wave functions of the N_q occupied states for the different particles $q = n, p, \Xi$ in a hypernucleus. The minimization of the total energy in Eq. (1) implies the SHF Schrödinger equation for each s.p. state (i, q) ,

$$\left[-\nabla \cdot \frac{1}{2m_q^*} \nabla + V_q(\mathbf{r}) - i\mathbf{W}_q(\mathbf{r}) \cdot (\nabla \times \boldsymbol{\sigma}) \right] \phi_q^i(\mathbf{r}) = e_q^i \phi_q^i(\mathbf{r}), \quad (3)$$

where the mean fields of nucleons and hyperon (including the Coulomb interaction) are written as

$$V_q = V_q^{\text{SHF}} + V_q^{(\Xi)}, \quad V_q^{(\Xi)} = \frac{\partial \varepsilon_{\Xi N}}{\partial \rho_q}, \quad (q = n, p), \quad (4)$$

$$V_{\Xi} = \frac{\partial \varepsilon_{\Xi N}}{\partial \rho_{\Xi}} - V_C. \quad (5)$$

The nucleonic spin-orbit mean field is represented by $\mathbf{W}_{n,p}$ and is provided by the NN Skyrme force used here, whereas we assume $\mathbf{W}_{\Xi} = 0$ in this work. For the nucleonic energy density functional ε_{NN} we employ the SLy4 parametrization [25, 28], while the energy density functional for the hyperonic part is given by [14, 24, 26],

$$\begin{aligned} \varepsilon_{\Xi N} = & \frac{\tau_{\Xi}}{2m_{\Xi}} + a_0 \rho_{\Xi} \rho_N + a_3 \rho_{\Xi} \rho_N^2 + a_1 (\rho_{\Xi} \tau_N + \rho_N \tau_{\Xi}) \\ & - a_2 (\rho_{\Xi} \Delta \rho_N + \rho_N \Delta \rho_{\Xi}) / 2 - a_4 (\rho_{\Xi} \nabla \cdot \mathbf{J}_N + \rho_N \nabla \cdot \mathbf{J}_{\Xi}), \end{aligned} \quad (6)$$

which provides the hyperonic SHF mean fields

$$V_{\Xi} = a_0 \rho_N + a_3 \rho_N^2 + a_1 \tau_N - a_2 \Delta \rho_N - a_4 \nabla \cdot \mathbf{J}_N, \quad (7)$$

$$V_N^{(\Xi)} = a_0 \rho_{\Xi} + 2a_3 \rho_N \rho_{\Xi} + a_1 \tau_{\Xi} - a_2 \Delta \rho_{\Xi} - a_4 \nabla \cdot \mathbf{J}_{\Xi}, \quad (8)$$

and a Ξ effective mass

$$\frac{1}{2m_{\Xi}^*} = \frac{1}{2m_{\Xi}} + a_1 \rho_N. \quad (9)$$

The relation to the standard ΞN Skyrme parameters $t_{0,1,2,3}^{\Xi N}$ is

$$a_0 = t_0, \quad a_1 = \frac{t_1 + t_2}{4}, \quad a_2 = \frac{3t_1 - t_2}{8}, \quad a_3 = \frac{3t_3}{8}. \quad (10)$$

Due to lack of experimental data for Ξ^- hypernuclei, three simple ΞN Skyrme forces SLX0, SLX2, SLX3 that employ no more than two parameters were proposed in Ref. [14]. (We use here the notation $\text{SLX}^* \equiv \text{SL}^*_p$ of that work). The SLX0 force involves only a volume term $\sim a_0$, while in SLX2 and SLX3 the parameters are chosen as $a_2 = 20 \text{ MeVfm}^5$ and $a_3 = 1000 \text{ MeVfm}^6$, respectively, motivated by $N\Lambda$ Skyrme forces [26]. The values of a_0 in SLX0, SLX2, SLX3 were fixed to $-128, -138, -228 \text{ MeVfm}^6$, respectively, reproducing the experimental data of $B_{\Xi} = 1.11 \pm 0.25 \text{ MeV}$ in the hypernucleus ${}^{15}_{\Xi}\text{C}$ with the Ξ^- hyperon occupying the $1p$ orbit. The SLX3 force then predicts also results compatible with the experimental information on ${}^{12}_{\Xi}\text{Be}$ [10].

In our approach, we assume axial symmetry of the mean field, and the deformed SHF Schrödinger equation is solved in cylindrical coordinates (r, z) within the axially-deformed harmonic-oscillator basis [23, 25]. This allows us to make calculations of 2D-deformed nuclei and hypernuclei. The quadrupole deformation parameter of the nuclear core is expressed as

$$\beta_2 \equiv \sqrt{\frac{\pi}{5}} \frac{\langle 2z^2 - r^2 \rangle}{\langle r^2 + z^2 \rangle}, \quad (11)$$

while the nuclear core radius is given by

$$R_N \equiv \sqrt{\langle r^2 + z^2 \rangle} = \sqrt{\frac{N}{A-1} \langle R_n^2 \rangle + \frac{Z}{A-1} \langle R_p^2 \rangle}. \quad (12)$$

The calculated results of these observables will be discussed in the next section, together with the Ξ^- separation energy

$$B_{\Xi} \equiv E[AZ] - E[A+1_{\Xi}(Z-1)], \quad (13)$$

in which notation Z is the charge number, and A is the total baryon number of a hypernucleus.

At the present stage of investigation we neglect the difference of the $\Xi^- p$ and $\Xi^- n$ interactions for the nearly symmetric nuclei we are considering here. Also, the imaginary part of the Ξ^- potential in our approach is currently neglected, because it is fairly small at low momenta, $\text{Im} U(k=0) / \text{Re} U(k=0) \approx 0.2$ in Brueckner-Hartree-Fock (BHF) calculations [27], where $\text{Im} U$ has a strong dependence on the coupling of the ΞN and $\Lambda\Lambda$ channels.

III. RESULTS

We now study systematically a series of single Ξ^- hypernuclei in the ground state (Ξs) and the first excited state (Ξp). Among them, the hypernuclei with spherical cores are ${}^{15}_{\Xi}\text{C}$, ${}^{17}_{\Xi}\text{N}$, ${}^{41}_{\Xi}\text{K}$, ${}^{91}_{\Xi}\text{Y}$, and ${}^{209}_{\Xi}\text{Ti}$; and the ones with deformed cores are ${}^9_{\Xi}\text{Li}$, ${}^{10}_{\Xi}\text{Li}$, ${}^{12}_{\Xi}\text{Be}$, ${}^{13}_{\Xi}\text{B}$, ${}^{21}_{\Xi}\text{F}$, and ${}^{37}_{\Xi}\text{Cl}$.

TABLE I. Deformation parameter β_2 , separation energy B_{Ξ^-} , and nuclear core radius R_N for several hypernuclei obtained with the SLX0, SLX2, and SLX3 forces. The subscripts s and p denote the orbit that the Ξ^- hyperon occupies. The B_{Ξ^-} values in brackets are the results of deformed SHF calculations without ΞN Coulomb interaction. Experimental data [8, 9, 13], and theoretical results of a cluster model calculation [11] and a RMF model [21] are listed for comparison.

	K^π	β_2				B_{Ξ^-} (MeV)			Data	R_N (fm)			
		no Ξ	SLX0	SLX2	SLX3	SLX0	SLX2	SLX3		no Ξ	SLX0	SLX2	SLX3
${}^9_{\Xi_s}\text{Li}$	$0^+ \otimes \Xi_{\frac{1}{2}}^{1+}$	0.622	0.589	0.591	0.616	3.6 (1.6)	2.8 (1.0)	3.5 (1.0)		2.548	2.477	2.492	2.558
${}^{10}_{\Xi_s}\text{Li}$	$n_{\frac{3}{2}}^- \otimes \Xi_{\frac{1}{2}}^{1+}$	0.373	0.259	0.264	0.358	5.2 (3.0)	4.6 (2.4)	4.1 (2.0)	3.6 (1.6) [11]	2.444	2.372	2.392	2.480
${}^{12}_{\Xi_s}\text{Be}$	$p_{\frac{3}{2}}^- \otimes \Xi_{\frac{1}{2}}^{1+}$	0.127	0.101	0.100	0.123	8.0 (5.1)	7.2 (4.4)	5.2 (2.6)	5 (2.2) [11]	2.436	2.385	2.399	2.456
${}^{13}_{\Xi_s}\text{B}$	$p_{\frac{3}{2}}^- \otimes \Xi_{\frac{1}{2}}^{1+}$	-0.302	-0.254	-0.254	-0.295	8.1 (4.8)	7.6 (4.3)	6.2 (3.2)		2.598	2.523	2.530	2.606
${}^{13}_{\Xi_p}\text{B}$	$p_{\frac{3}{2}}^- \otimes \Xi_{\frac{3}{2}}^{1+}$	-0.302	-0.311	-0.310	-0.318	0.4	0.3	0.7	0.82 ± 0.17 [8]	2.598	2.598	2.597	2.622
${}^{15}_{\Xi_s}\text{C}$	$p_{\frac{1}{2}}^- \otimes n_{\frac{1}{2}}^- \otimes \Xi_{\frac{1}{2}}^{1+}$	0	0	0	0	10.4 (6.5)	10.0 (6.1)	7.2 (3.7)	9.4 (5.7) [21]	2.582	2.539	2.545	2.597
${}^{15}_{\Xi_p}\text{C}$	$p_{\frac{1}{2}}^- \otimes n_{\frac{3}{2}}^- \otimes \Xi_{\frac{3}{2}}^{1+}$	0	-0.020	-0.020	-0.010	1.1	1.1	1.1	1.11 ± 0.25 [9, 13]	2.582	2.572	2.576	2.592
${}^{17}_{\Xi_s}\text{N}$	$0^+ \otimes \Xi_{\frac{1}{2}}^{1+}$	0	0	0	0	11.2 (6.9)	11.0 (6.7)	8.1 (4.2)	8.1 [21]	2.674	2.634	2.639	2.686
${}^{17}_{\Xi_p}\text{N}$	$0^+ \otimes \Xi_{\frac{3}{2}}^{1+}$	0	-0.005	-0.005	-0.004	2.2	2.2	2.0	2.1 [21]	2.674	2.660	2.664	2.683
${}^{21}_{\Xi_s}\text{F}$	$0^+ \otimes \Xi_{\frac{1}{2}}^{1+}$	0.394	0.381	0.381	0.390	13.4 (8.2)	13.3 (8.2)	9.5 (4.8)		2.925	2.880	2.882	2.936
${}^{21}_{\Xi_p}\text{F}$	$p_{\frac{1}{2}}^- \otimes \Xi_{\frac{3}{2}}^{1+}$	0.394	0.377	0.377	0.381	3.5	3.6	3.1		2.925	2.903	2.904	2.926
${}^{37}_{\Xi_s}\text{Cl}$	$0^+ \otimes \Xi_{\frac{1}{2}}^{1+}$	-0.151	-0.139	-0.139	-0.154	20.4 (12.0)	20.9 (12.5)	13.9 (6.2)		3.309	3.276	3.276	3.322
${}^{37}_{\Xi_p}\text{Cl}$	$p_{\frac{1}{2}}^- \otimes \Xi_{\frac{3}{2}}^{1+}$	-0.151	-0.158	-0.158	-0.154	12.4 (4.8)	12.6 (5.0)	9.3 (2.3)		3.309	3.293	3.293	3.318
${}^{41}_{\Xi_s}\text{K}$	$0^+ \otimes \Xi_{\frac{1}{2}}^{1+}$	0	0	0	0	20.8 (11.7)	21.4 (12.3)	14.4 (6.1)	16.6 [21]	3.396	3.368	3.368	3.406
${}^{41}_{\Xi_p}\text{K}$	$0^+ \otimes \Xi_{\frac{3}{2}}^{1+}$	0	-0.003	-0.003	-0.001	12.8 (4.5)	13.1 (4.9)	9.6 (2.1)	10.5 [21]	3.396	3.377	3.379	3.394
${}^{91}_{\Xi_s}\text{Y}$	$0^+ \otimes \Xi_{\frac{1}{2}}^{1+}$	0	0	0	0	30.0 (15.3)	31.1 (16.3)	21.8 (8.0)	23.0 [21]	4.261	4.236	4.240	4.264
${}^{91}_{\Xi_p}\text{Y}$	$0^+ \otimes \Xi_{\frac{3}{2}}^{1+}$	0	0.003	0.003	0.003	24.2 (10.2)	25.0 (11.0)	18.0 (5.1)	17.9 [21]	4.261	4.246	4.246	4.270
${}^{209}_{\Xi_s}\text{Ti}$	$0^+ \otimes \Xi_{\frac{1}{2}}^{1+}$	0	0	0	0	37.0 (13.4)	38.1 (14.5)	28.6 (5.7)	29.7 [21]	5.538	5.524	5.527	5.540
${}^{209}_{\Xi_p}\text{Ti}$	$0^+ \otimes \Xi_{\frac{3}{2}}^{1+}$	0	0.001	0.001	0.001	32.8 (10.0)	33.9 (11.2)	25.5 (3.6)	26.3 [21]	5.538	5.526	5.530	5.542

A. Radii

In Table I we list the calculated values of the deformation parameter β_2 , the Ξ^- separation energy B_{Ξ^-} , and the nuclear core radius R_N for the different Ξ^- hypernuclei. It is found that the core radius of a Ξ^- hypernucleus generally decreases compared to that of the core nucleus with the SLX0 and SLX2 forces, but slightly increases with the SLX3. This modification of the core size is larger when the Ξ^- hyperon occupies the concentrated $1s$ state than the more diluted $1p$ state.

This is because the magnitude of the deformation change is determined by the competition between the attractive linear term ($\sim a_0$) and the repulsive nonlinear term ($\sim a_3$) of the hyperonic SHF mean field Eq. (7), and thus depends on the ΞN force, see Fig. 1 of [14]. The SLX3 force features strongest attraction at low density in the peripheral region ($\rho_N \approx 0.1 \text{ fm}^{-3}$) of the core nucleus, but much less at the higher central density and thus tends to dilute the core, whereas SLX0 or SLX2 exhibit the opposite behavior and contract the core. For better illustration we plot in Fig. 1 the radius change

$$\delta R_N \equiv R_N[AZ] - R_N[A+1_{\Xi}(Z-1)], \quad (14)$$

for the different nuclei, confirming the qualitative difference between the XNI forces explained above, namely, positive values of δR_N with SLX3 and negative values with SLX0 or

SLX2. Moreover, the core radius changes are naturally largest for small nuclei.

B. Removal energies

These properties also influence the removal energies B_{Ξ^-} listed in the table: Apart from the weakly bound ${}^{15}_{\Xi_p}\text{C}$, where all forces yield by construction the same $B_{\Xi^-} = 1.1 \text{ MeV}$, the SLX3 force predicts generally smaller B_{Ξ^-} values than SLX0 and SLX2 for larger and stronger bound hypernuclei, where the relevant central high-density nuclear domain is more extended. This feature allowed also the best fit of the experimental data for the hypernucleus ${}^{12}_{\Xi_s}\text{Be}$ among the SLX* forces [14]. The Ξ^- binding energies obtained by SLX3 are close to the results of the RMF model [21] as well.

However, for weakly bound hypernuclei like ${}^{15}_{\Xi_p}\text{C}$, where a low-density nuclear environment prevails for the Ξ^- , the situation is opposite, in particular we notice that the Ξ^- removal energy of the deformed nucleus ${}^{13}_{\Xi_p}\text{B}$ derived with SLX3 is 0.7 MeV, larger than that of the other two forces. This value is consistent with the experimental data of $0.82 \pm 0.17 \text{ MeV}$ in the E176 experiment [8, 9]. (The Ξ^- hyperon occupies the $1p_{3/2}$ state. In our model, the $[110]1/2^-$ and $[101]3/2^-$ orbits are the same without hyperon spin-orbit coupling, but the $[101]1/2^-$ orbit is separated due to the nuclear deformation).

In order to illustrate this hypernucleus in more detail, we

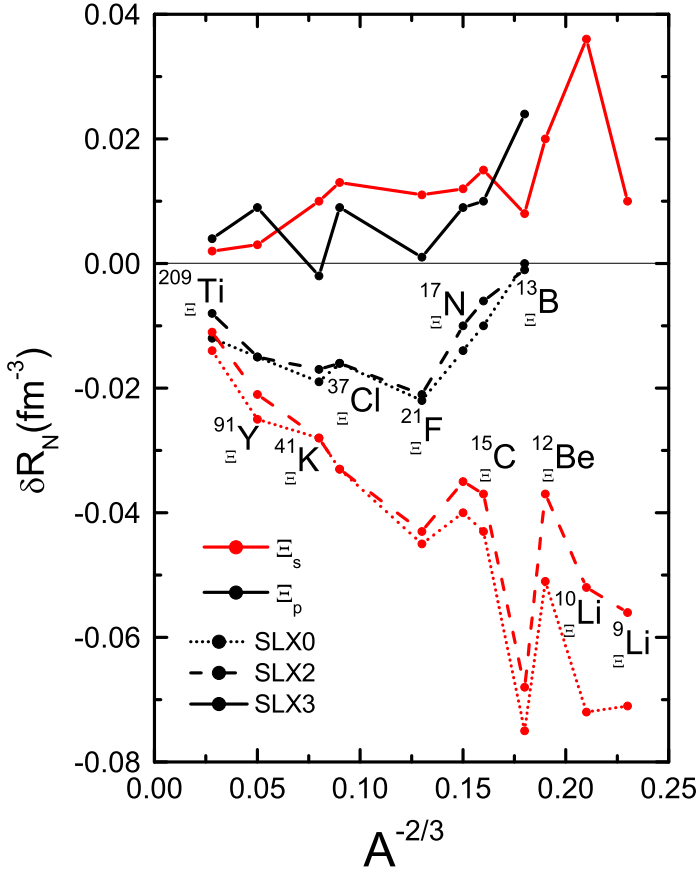


FIG. 1. Core radius change δR_N , Eq. (14), for several nuclei, obtained with different ΞN forces. The subscripts s and p denote the Ξ^- orbit.

plot in Fig. 2 the Ξ^- potential (upper panel) and the N , Ξ density distributions (lower panel). With the SLX0,2,3 forces, the depth of $V_{\Xi}(r=0)$ is about 23, 24, 15 MeV. However, the width of the SLX3 potential is larger, thus providing more binding for the hyperon in the extended p orbit: It is seen in the lower panel that the major part of the kaon is located in the range $r \gtrsim 2.5$ fm, where the SLX3 potential is deeper than those of SLX0, SLX2.

We notice another related interesting phenomenon regarding the Ξ^- removal energy of deformed hypernuclei, namely the results of B_{Ξ} are different for deformed and undeformed calculations. The quantity

$$\Delta B_{\Xi} \equiv B_{\Xi}^{\text{def.}} - B_{\Xi}^{\text{nondef.}} \quad (15)$$

is listed in Table II for various hypernuclei with sizeable deformations. It is seen that the Ξ^- hyperon in the $1s$ state is bound less in deformed nuclei than the same undeformed ones, which is caused by a reduction of the mean nucleon density in the former case. However, for the p -state Ξ^- hypernuclei with oblate deformation like ${}_{\Xi p}^{13}\text{B}$ and ${}_{\Xi p}^{37}\text{Cl}$, the effect is opposite. In these two hypernuclei, the Ξ^- hyperon occupying the extended $1p$ orbit is more bound due to the core deformation, which might actually increase the density in the peripheral part where the hyperon resides. In particular, the ${}_{\Xi p}^{13}\text{B}$ hypernucleus calculated by the 1D model is unbound with

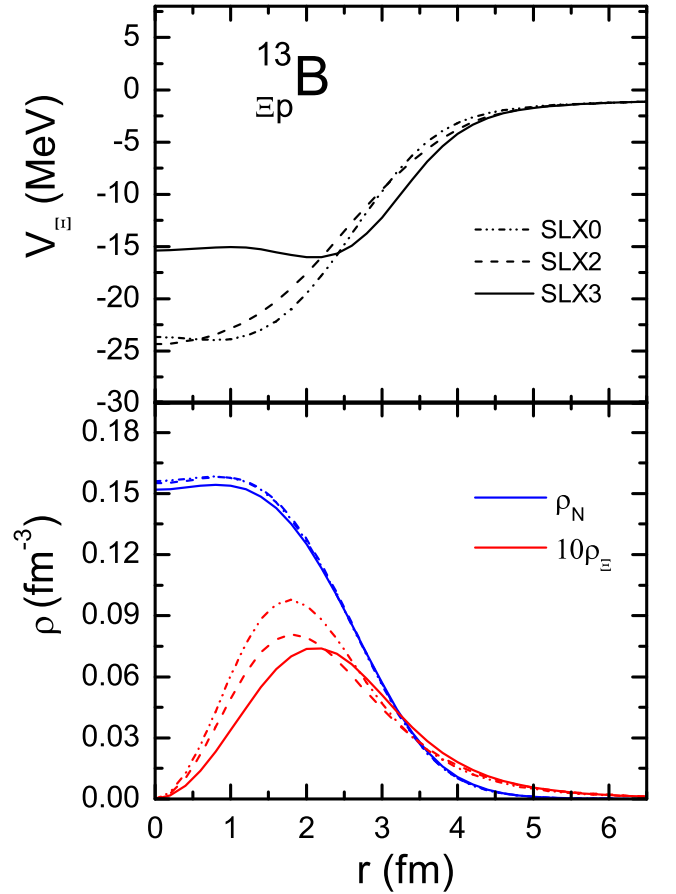


FIG. 2. The mean field potential V_{Ξ} (upper panel) and the N , Ξ densities (lower panel) in the hypernucleus ${}_{\Xi p}^{13}\text{B}$ calculated with different ΞN forces.

$B_{\Xi} = -0.27, -0.25, 0.06$ MeV in the cases of SLX0, SLX2, and SLX3, respectively, while in the 2D approach it becomes bound with $B_{\Xi} = 0.43, 0.27, 0.68$ MeV. On the contrary, in the prolately deformed hypernucleus ${}_{\Xi p}^{21}\text{F}$, the overlap of the p -state Ξ^- hyperon with the prolate core is weaker than in the undeformed case, and therefore it is also less bound in the 2D model.

C. Deformation

To study in more detail the effect of a single Ξ^- hyperon on the nuclear core deformation, we plot in Fig. 3 the binding energy surfaces (BESs) of the core nuclei ${}^8\text{Be}$, ${}^{11}\text{B}$, ${}^{12}\text{C}$, ${}^{20}\text{Ne}$, and their Ξ^- hypernuclei ${}_{\Xi s}^9\text{Li}$, ${}_{\Xi s}^{12}\text{Be}$, ${}_{\Xi p}^{13}\text{B}$, ${}_{\Xi p}^{21}\text{F}$. In order to better compare the curves, the BESs of the Ξ^- hypernuclei are shifted by a constant amount so as to obtain the same minimum value. The corresponding values of β_2 at minimum are listed in Table I. We observe that for the three light nuclei the addition of the Ξ^- makes the energy minima more pronounced whether the curve has one single or two minima. In the latter case, an eventual second minimum becomes more shallow (a) or disappears entirely (c). For ${}_{\Xi p}^{21}\text{F}$ (d) instead, the

TABLE II. The difference between the 2D and 1D calculations of the Ξ^- removal energy, $\Delta B_{\Xi} = B_{\Xi}^{(2D)} - B_{\Xi}^{(1D)}$, for several deformed nuclei with different ΞN forces.

	β_2	ΔB_{Ξ} (MeV)		
	no Ξ	SLX0	SLX2	SLX3
${}^9_{\Xi_s}\text{Li}$	0.62	-0.70	-0.63	-0.08
${}^{10}_{\Xi_s}\text{Li}$	0.37	-0.25	-0.24	-0.02
${}^{12}_{\Xi_s}\text{Be}$	0.13	-0.05	-0.05	0.00
${}^{13}_{\Xi_s}\text{B}$	-0.30	-0.51	-0.49	0.00
${}^{13}_{\Xi_p}\text{B}$	-0.30	0.70	0.52	0.62
${}^{21}_{\Xi_s}\text{F}$	0.39	-0.19	-0.27	-0.16
${}^{21}_{\Xi_p}\text{F}$	0.39	-1.13	-1.02	-0.70
${}^{37}_{\Xi_s}\text{Cl}$	-0.15	-0.27	-0.25	-0.05
${}^{37}_{\Xi_p}\text{Cl}$	-0.15	0.35	0.34	0.27

depth of the second minimum increases.

These effects can be understood by analyzing the overlap of the density distribution of the added Ξ^- hyperon with the nucleon density distributions of configurations of various shapes, which determines the energy gain by the added hyperon. For example, returning to the case of ${}^{13}_{\Xi_p}\text{B}$ in panel (c), one observes that due to the overlap of the Ξ^- density distribution and the deformed nucleon distribution the total energy is lowered for oblate configurations but increased for prolate ones. Consequently the existing oblate minimum becomes even more pronounced. The same effect is exhibited for ${}^{21}_{\Xi_p}\text{F}$ (d), where the second, oblate, minimum becomes deeper when adding the p -state hyperon.

For the light nucleus ${}^9_{\Xi_s}\text{Li}$ (a), we notice that the BESs by the three forces show visible differences, particularly for SLX3, whose curve has the most pointed minimum compared to the other two curves. In this case of a centered Ξ^- , the nucleonic environment of the prolate configuration is more advantageous than the oblate one, such that the existing minimum is also deepened here.

D. Densities

More information on the nucleon and hyperon density distributions is given in Fig. 4, which shows those of the hypernucleus ${}^{15}_{\Xi}\text{C}$ obtained with the different XNIs. Consistent with the analysis of the nuclear radii in Table I, one observes that the central nucleon density $\rho_N(r=0)$ in hypernuclei calculated by SLX0 and SLX2 is larger than that in the core nuclei (core shrinking), while the opposite occurs with the force SLX3 (core expansion). For the p -state hypernucleus ${}^{15}_{\Xi_p}\text{C}$, the effect is reduced due to the vanishing of the hyperon density in the core, and consequently in Fig. 4 with the SLX3 force, the central nucleon density of the p -state hypernuclei is larger than that of the s -state hypernuclei, while all forces make more nucleons reside in the peripheral region ($r \gtrsim 2$ fm) of p -state hypernuclei.

These modifications of the nucleonic density can be un-

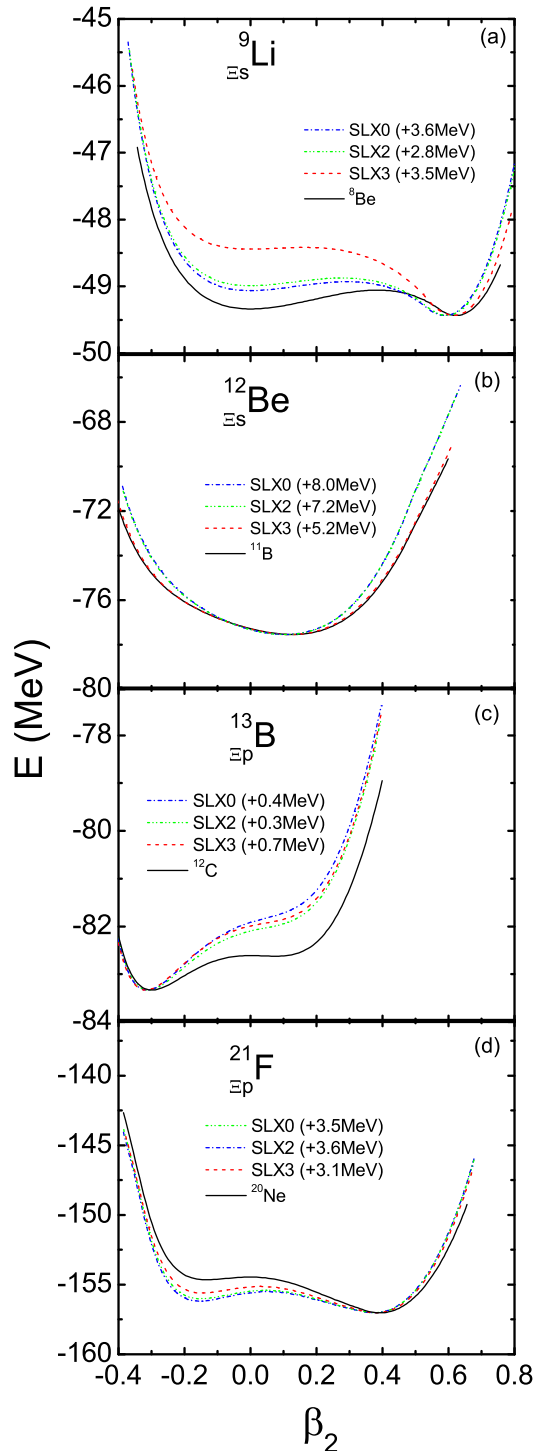


FIG. 3. The binding energy surfaces obtained with different ΞN forces for (a) ${}^8\text{Be}$ and ${}^9_{\Xi_s}\text{Li}$; (b) ${}^{11}\text{B}$ and ${}^{12}_{\Xi_s}\text{Be}$; (c) ${}^{12}\text{C}$ and ${}^{13}_{\Xi_p}\text{B}$; (d) ${}^{20}\text{Ne}$ and ${}^{21}_{\Xi_p}\text{F}$.

derstood by the hyperonic part of the nucleon mean field $V_N^{(\Xi)} \sim (a_0 + 2a_3\rho_N)\rho_{\Xi}$, which due to the competition between the attractive a_0 and repulsive a_3 components for the SLX3 force is repulsive at the center and attractive in the peripheral region ($r \gtrsim 2$ fm) of the ${}^{15}_{\Xi}\text{C}$ nucleus, as shown in Fig. 5.

Consistent effects on the hyperon density are observed in

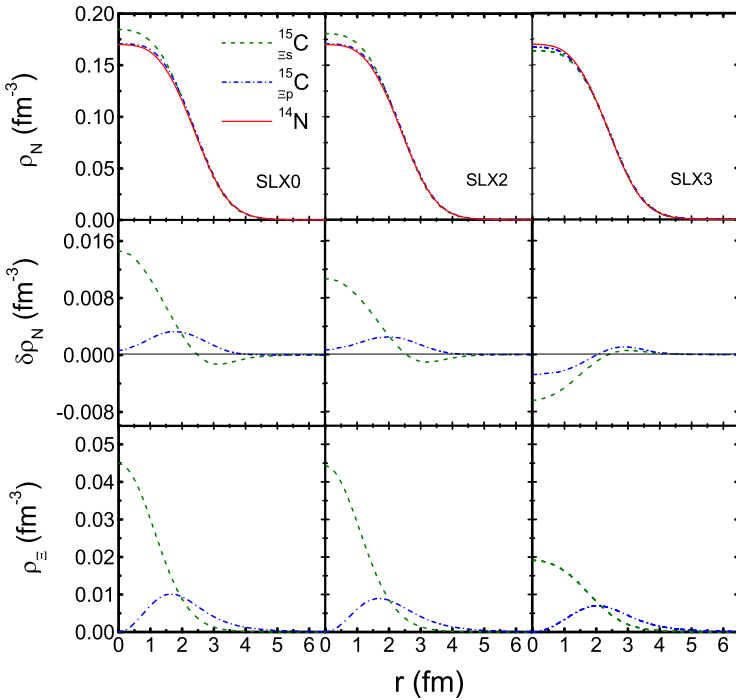


FIG. 4. Nucleon and hyperon density distributions of $^{15}_{\Xi s}\text{C}$, $^{15}_{\Xi p}\text{C}$, and the core nucleus ^{14}N , obtained with different ΞN forces. $\delta\rho_N$ is the change of the nucleon density by the added hyperon. The subscripts s and p denote the Ξ^- orbit.

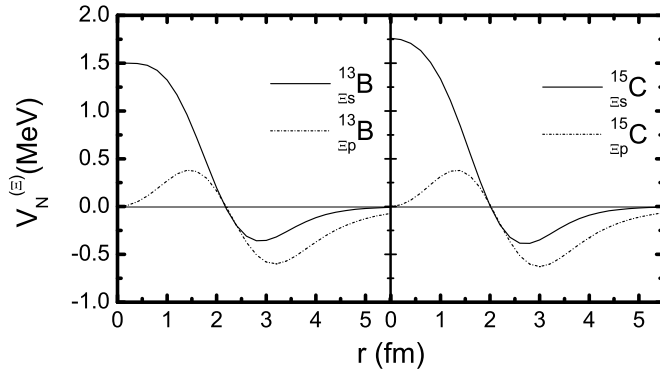


FIG. 5. The hyperonic contribution to the nucleon mean field $V_N^{(\Xi)}$, Eq. (8), for the s - or p -state hypernuclei $^{13}_{\Xi}\text{B}$ and $^{15}_{\Xi}\text{C}$ with the SLX3 force.

the lower panel of Fig. 4, namely the hyperon density is more spread out and smaller in the center with the force SLX3 than with the other two forces. On a reduced scale, these effects also take place in the heavier hypernuclei examined.

E. Ξ^- binding

Finally, Figure 6 summarizes the mass dependence of the hyperon removal energies obtained with three XNIs SLX0, SLX2 and SLX3, including or not the ΞN Coulomb interaction, which becomes increasingly important for the heavier nuclei due to its long-range nature. For heavy nuclei the

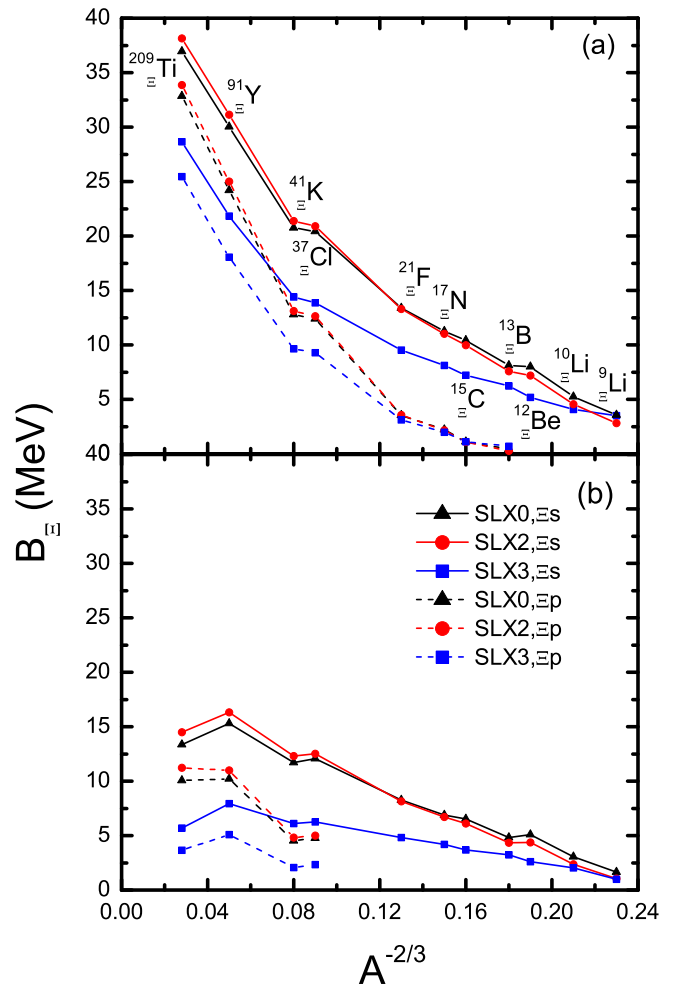


FIG. 6. Hyperon binding energies B_{Ξ} as a function of mass number $A^{-2/3}$ with different ΞN forces and with (a) or without (b) ΞN Coulomb potential.

sults with the full interaction approach about 30 MeV with the SLX3 force, which is very similar to the case of Λ hypernuclei [26]. Due to the missing repulsive contribution at normal density, the SLX0 or SLX2 force yield about 10 MeV more binding for heavy nuclei.

IV. CONCLUSIONS

We systematically studied hyperon removal energies, nuclear core radii, core deformations, and density distributions of Ξ^- hypernuclei using a 2D SHF model with three different ΞN Skyrme forces adjusted to reproduce experimental data for $^{15}_{\Xi p}\text{C}$.

The SLX3 ΞN force is the only one to yield simultaneous agreement with the $^{12}_{\Xi s}\text{Be}$ data. It incorporates an important density-dependent repulsive component and thus yields maximum attraction at subnuclear densities. Consequently the induced core deformation is a dilatation and the Ξ^- binding energies of heavy nuclei obtained with SLX3 are smaller than those with the other forces, and more similar to those of RMF

or cluster model calculations.

The hyperon removal energy of ${}_{\Xi p}^{13}\text{B}$ with the SLX3 force is 0.7 MeV, compatible with a possible value of 0.82 ± 0.17 MeV interpreted from the KEK E176 experiment. We thus predict that this system is a possibly bound p -state Ξ^- hypernucleus. But still more accurate experiments are needed to confirm the reliability of the observed event. Also, the prediction of this weakly bound state is delicate, as it depends on the nuclear deformation: This hypernucleus is unbound in the 1D model, but bound in the 2D model due to its more extended geometry favoring lower and more attractive nuclear densities.

This feature was studied in detail analyzing the nuclear core radii and density distributions of several Ξ^- hypernuclei. Due to their different density dependence, the three ΞN Skyrme forces impose different variations on the nucleon density compared to that of the core nuclei: With SLX0 or SLX2, the central nucleon density increases, while it decreases with SLX3 due to a repulsive effect on the nucleons in the central region of nuclei. This leads to a contraction/dilatation of the core, respectively.

These differences also influence the BESs of the various nuclei, and we have pointed out the delicate interplay between Ξ^- s or p state occupation and the prolate or oblate nuclear environment, which modifies the minima of the BES.

In this context we remark, however, that the mean-field ap-

proximation employed here might be inadequate in particular for weak BES minima, due to the neglect of configuration mixing. A beyond-mean-field treatment [29, 30] might be required for a more realistic modelling in the future.

Finally, we studied the mass dependence of the Ξ^- binding energies in a broad region of the mass table and predict removal energies of about 30 MeV for the heaviest hypernuclei with the SLX3 force.

We hope that our calculations and predictions can help to identify the bound Ξ^- hypernuclei. Currently, there are several projects for measuring Ξ^- hypernuclei and Ξ^- atoms by upgraded technologies at J-PARC and other facilities. In the future, more reliable and accurate experimental data on Ξ^- hypernuclei will become available and provide more constraints on the ΞN interaction. This will allow to determine more precisely the parameters of the ΞN Skyrme force and permit more accurate predictions.

ACKNOWLEDGMENTS

We thank Ji-Wei Cui for suggestive discussions. This work was supported by the National Science Foundation of China under contract No. 11775081, and the Natural Science Foundation of Shanghai under contract No. 17ZR1408900.

-
- [1] O. Hashimoto and H. Tamura, *Prog. Part. Nucl. Phys.* **57**, 564 (2006); A. Feliciello and T. Nagae, *Rep. Prog. Phys.* **78**, 096301 (2015); A. Gal, E. V. Hungerford, and D. J. Millener, *Rev. Mod. Phys.* **88**, 035004 (2016).
 - [2] J. Schaffner-Bielich, *Nucl. Phys.* **A804**, 309 (2008); **A835**, 279 (2010).
 - [3] M. Danysz and J. Pniewski, *Philos. Mag.* **44**, 348 (1953).
 - [4] K. Tanida et al., http://j-parc.jp/researcher/Hadron/en/pac_0606/pdf/p0606_tanida.pdf.
 - [5] K. Imai et al., http://j-parc.jp/researcher/Hadron/en/pac_0606/pdf/p0606_ima.pdf.
 - [6] S. Aoki et al., *Prog. Theor. Phys.* **89**, 493 (1993); S. Aoki et al., *Phys. Lett.* **B355**, 45 (1995).
 - [7] M. Yamaguchi, K. Tominaga, Y. Yamamoto, and T. Ueda, *Prog. Theor. Phys.* **105**, 627 (2001).
 - [8] S. Aoki et al., *Nucl. Phys.* **A828**, 191 (2009).
 - [9] K. Nakazawa et al., *Prog. Theor. Exp. Phys.* 033D02 (2015).
 - [10] P. Khaustov, D.E. Alburger, P. D. Barnes, B. Bassalleck, A.R. Berdoz, A. Biglan, T. Burger, D. S. Carman, R. E. Chrien et al. (AGS E885 collaboration), *Phys. Rev.* **C61**, 054603 (2000).
 - [11] E. Hiyama, Y. Yamamoto, T. Motoba, Th. A. Rijken, and M. Kamimura, *Phys. Rev.* **C78**, 054316 (2008).
 - [12] H. Matsumiya, K. Tsubakihara, M. Kimura, A. Dote, and A. Ohnishi, *Phys. Rev.* **C83**, 024312 (2011).
 - [13] K. Nakazawa (private communication).
 - [14] T. T. Sun, E. Hiyama, H. Sagawa, H.-J. Schulze, and J. Meng, *Phys. Rev.* **C94**, 064319 (2016).
 - [15] T. Nagae et al. (J-PARC E05 collaboration), *AIP Conference Proceedings* **2130**, 020015 (2019).
 - [16] S. Acharya et al., *Phys. Rev. Lett.* **123**, 112002 (2019).
 - [17] E. Hiyama and K. Nakazawa, *Ann. Rev. Nucl. Part. Sci.* **68**, 131 (2018).
 - [18] J. Mareš and B. K. Jennings, *Phys. Rev.* **C49**, 2472 (1994).
 - [19] Y. H. Tan and P. Z. Ning, *Eur. Phys. J. A* **20**, 257 (2004).
 - [20] Z.-X. Liu, C.-J. Xia, W.-L. Lu, Y.-X. Li, J. N. Hu, and T.-T. Sun, *Phys. Rev.* **C98**, 024316 (2018).
 - [21] T. Nakazawa and H. Shen, *Phys. Rev.* **C96**, 054304 (2017).
 - [22] T. Nakazawa and D. M. Brink, *Phys. Rev.* **C5**, 626 (1972).
 - [23] D. Vautherin, *Phys. Rev.* **C7**, 296 (1973).
 - [24] M. Rayet, *Ann. Phys. (N.Y.)* **102**, 226 (1976); *Nucl. Phys.* **A367**, 381 (1981).
 - [25] M. Bender, P.-H. Heenen, and P.-G. Reinhard, *Rev. Mod. Phys.* **75**, 121 (2003); J. R. Stone and P.-G. Reinhard, *Prog. Part. Nucl. Phys.* **58**, 587 (2007); J. Erler, P. Klüpfel, and P.-G. Reinhard, *J. Phys. G: Nucl. Part. Phys.* **38**, 033101 (2011).
 - [26] H.-J. Schulze and E. Hiyama, *Phys. Rev.* **C90**, 047301 (2014).
 - [27] H.-J. Schulze and T. Rijken, *Phys. Rev.* **C88**, 024322 (2013); Th.A. Rijken and H.-J. Schulze, *Eur. Phys. J. A* **52**, 21 (2016).
 - [28] E. Chabanat, P. Bonche, P. Haensel, J. Meyer, and R. Schaeffer, *Nucl. Phys.* **A627**, 710 (1997); **A635**, 231 (1998); **A643**, 441 (1998).
 - [29] J.-W. Cui, X.-R. Zhou, L.-X. Guo, and H.-J. Schulze, *Phys. Rev.* **C95**, 024323 (2017); J.-W. Cui and X.-R. Zhou, *PTEP* **9**, 093D04 (2017); W.-Y. Li, J.-W. Cui, and X.-R. Zhou, *Phys. Rev.* **C97**, 034302 (2018).
 - [30] H. Mei, K. Hagino, J. M. Yao, and T. Motoba, *Phys. Rev.* **C97**, 064318 (2018).